Monte Carlo simulations of disorder in $ZnSnN_2$ and the effects on the electronic structure

Stephan Lany,[1] Angela N. Fioretti,[1,2] Paweł P. Zawadzki,[1] Laura T. Schelhas,[3] Eric S. Toberer,[1,2] Andriy Zakutayev,[1] and Adele C. Tamboli[1,2]

[1]*National Renewable Energy Laboratory, Golden, Colorado 80401, USA*

[2]*Colorado School of Mines, Golden, Colorado 80401, USA*

[3]*Applied Energy Programs, SLAC National Accelerator Laboratory, Menlo Park, California 94025, USA*

(Received 31 May 2017; published 10 August 2017)

In multinary compound semiconductors, cation disorder can decisively alter the electronic properties and impact potential applications. $ZnSnN_2$ is a ternary nitride of interest for photovoltaics, which forms in a wurtzite-derived crystal structure. In the ground state, every N anion is coordinated by two Zn and two Sn cations, thereby observing the octet rule locally. Using a motif-based model Hamiltonian, we performed Monte Carlo simulations that provide atomistic representations of $ZnSnN_2$ with varying degrees of cation disorder. Subsequent electronic structure calculations describe the evolution of band gaps, optical properties, and carrier localization effects as a function of the disorder. We find that octet-rule conserving disorder is practically impossible to avoid but perfectly benign, with hardly any effects on the electronic structure. In contrast, a fully random cation distribution would be very detrimental, but fortunately it is energetically highly unfavorable. A degree of disorder that can realistically be expected for nonequilibrium thin-film deposition leads to a moderate band-gap reduction and to moderate carrier localization effects. Comparing the simulated structures with experimental samples grown by sputtering, we find evidence that these samples indeed incorporate a certain degree of octet-rule violating disorder, which is reflected in the x-ray diffraction and in the optical absorption spectra. This study demonstrates that the electronic properties of $ZnSnN_2$ are dominated by changes of the local coordination environments rather than long-range ordering effects.

DOI: 10.1103/PhysRevMaterials.1.035401

Ternary and quaternary semiconductors are of high interest in photovoltaics, including $CuInSe_2$ [1], Cu_2ZnSnS_4 [2], and, more recently, $ZnSnN_2$ as an earth-abundant photovoltaic absorber [3–5]. In the ground-state structure, the Zn and Sn cations are predicted to be ordered in a specific fashion so as to minimize the total energy. However, disorder on the cation lattice can occur either thermodynamically [6] or due to growth by nonequilibrium deposition techniques [7]. Such disorder can have a profound effect on the electronic and optical properties [6,8–10]. In its simplest form, disorder can be described in terms of cation exchange defects, e.g., $Cu_{Zn} + Zn_{Cu}$ in Cu_2ZnSnS_4 [11], or $Zn_{Ge} + Ge_{Zn}$ in $ZnGeN_2$ [10]. As a more general formulation, we introduced in Ref. [9] a model Hamiltonian expressing the energy in terms of anion-centered motifs, thereby describing the enthalpy change in Cu_2SnS_3 and Cu_2ZnSnS_4 due to deviations from the cation ordering in the ground state. In examining the effect of disorder on the electronic properties of $ZnSnN_2$, the current literature has considered two extreme limits, i.e., fully random cation disorder [8], modeled via a special quasirandom structure (SQS) [12], and a minimum level of disorder in which the local octet rule is maintained [13]. While the random alloy approximation works often well for isovalent alloys, e.g., in III-V systems with Al^{3+} and Ga^{3+}, one should generally expect significant (nonrandom) short-range order effects in heterovalent systems (here, Zn^{2+} and Sn^{4+}) due to electrostatic interactions. Therefore, we aim to bridge the gap between these two limits by using the motif-based model Hamiltonian in conjunction with Monte Carlo simulations to generate atomic structures with different degrees of disorder. Subsequent band-gap-corrected electronic structure calculations describe the evolution of the electronic structure with an increasing level of disorder, yielding the dependence of the band gap, optical absorption, and the density of states. The latter is used to calculate the inverse participation ratio [14], describing the localization of the electronic states throughout the energy spectrum.

Monte Carlo simulations. The orthorhombic (ORC) ground-state crystal structure with the space group (SG) 33 of $ZnSnN_2$ can be derived from the tetrahedrally coordinated wurtzite structure, similarly to $ZnGeN_2$ [15]. Hence, the motif-based model Hamiltonian introduced in Ref. [9] expands the energy as

$$\Delta H = 2 \sum_{i,j} e_{i,j} n_{i,j}, \tag{1}$$

where $n_{i,j}$ counts the number of N-Zn_iSn_j tetrahedral motifs ($0 \leqslant i \leqslant 4$ and $j = 4 - i$). The ground-state structure consists of octet-rule conserving Zn_2Sn_2 motifs only (see inset in Fig. 1). The parameters $e_{i,j}$ were calculated using a least-squares fit to the density functional theory (DFT) energies of fifty 64-atom structures with randomly distributed cations with equal numbers of Zn and Sn. Since we are only considering energy differences between the same chemical compositions on the same underlying wurtzite structure, we can expect a good error cancellation of the DFT energies [16], providing accurate enthalpy differences. To estimate the error of the model Hamiltonian fit we performed crossvalidation with ten iterations and randomly split data into train (80%) and test (20%) sets. The resulting mean absolute error is 7.6 meV/atom. To calculate the equilibrium cation distribution, we performed Metropolis Monte Carlo (MC) simulations in 128 atom cells. This cell size was chosen so that the samples generated by the MC simulation are still suitable for subsequent calculations of the electronic structure properties

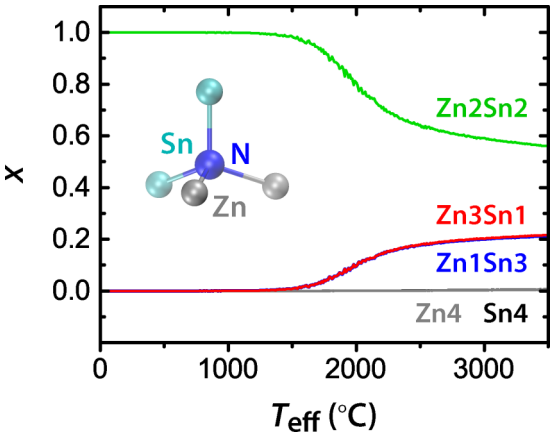

FIG. 1. Dependence of the concentration x of $Zn_{4-i}Sn_i$ motifs as a function of the effective temperature. The insert illustrates the cation coordination of the N-centered motifs using the octet-rule conserving Zn_2Sn_2 motif as an example.

(band gaps, density of states, absorption spectra). The cation distribution was randomly initialized, equilibrated at 3500 °C, and subsequently cooled using 10^4 MC steps per Kelvin. In the following, we discuss the temperature dependence of the fractional motif concentration $x_{ij} = n_{ij}/N_N$, where N_N is the total number of nitrogen sites per unit cell.

At around 2000 °C, we observe a transition from the octet-rule conserving Zn_2Sn_2 motif towards a partial disproportionation into Zn_3Sn_1 and Zn_1Sn_3 motifs. The Zn_4 and Sn_4 motifs are energetically unfavorable and do not occur in appreciable concentrations. The temperatures required to generate these non-ground-state motifs are far above the typical temperatures used for synthesis of $ZnSnN_2$ [5,8,17–19], which are below 600 °C. Due to the marginal thermodynamic stability of $ZnSnN_2$ (the formation enthalpy is calculated as $\Delta H_f = -0.13$ eV/fu), synthesis becomes difficult at higher temperatures and $ZnSnN_2$ will begin to decompose into the metals and N_2 gas. However, the temperature scale of Fig. 1 should be understood as an effective temperature measuring the degree of disorder resulting from nonequilibrium growth. In other words, the lack of equilibration during low-temperature growth results in a higher degree of randomness in the cation distribution than expected from fully equilibrated thermodynamics. In vapor-liquid-solid–grown $ZnGeN_2$, it was observed that the degree of ordering increased with increasing growth temperature and with annealing, indicating the initial kinetic trapping of a more random nonequilibrium state [20]. Techniques like pulsed laser deposition and sputtering can be even farther from equilibrium. The concept of effective temperature can be used to characterize this nonequilibrium randomness. For example, the analysis of Co_2ZnO_4 and Co_2NiO_4 films grown by pulsed laser deposition at 350 °C in a previous study has resulted in effective temperatures in the order of $T_{eff} = 2000$ °C [7]. Thus, for thin films grown by sputtering up to 400 °C, it is not unreasonable to expect fractions of Zn_3Sn_1 and Zn_1Sn_3 motifs around $x_{31} \approx x_{13} \approx 0.1$ (see Fig. 1). On the other hand, careful equilibration at elevated temperatures below the point of decomposition should enable the reduction or even elimination of these octet-rule violating motifs, since their concentration is insignificant below an effective temperature of 1000 °C (Fig. 1). We should emphasize that the effective temperature is a descriptor governing the configurational entropy of disorder, but vibrational entropy effects are limited due to the moderate actual deposition temperatures. Also, since we are considering only different atomic arrangements at the same composition and in the same tetrahedral bonding environment, vibrational effects are not expected to contribute significantly to the free energy difference.

Atomic structure. According to Quayle *et al.* [13], the octet-rule conserving Zn_2Sn_2 coordination can be realized in two wurtzite-derived orthorhombic crystal structures with smaller unit-cell sizes, i.e., a space group 33 ($Pna2_1$) structure with 16 atoms in the primitive cell and space group 26 ($Pmc2_1$) structure with an eight-atom cell. In larger cells, more arrangements are possible due to different stacking of rows of alternating Zn and Sn cations in the basal plane [13]. Apart from the 8- and 16-atom primitive cells, the Monte Carlo simulations also found a SG 33 structure with 32 atoms in the primitive cell that contain only Zn_2Sn_2 motifs. The DFT energies of all octet-rule conserving structures are very close, within 1.5 meV/atom, with the 16 atom SG33 structure having the lowest energy. For octet-rule violating disorder, we selected five samples each for a number $n = n_{31} = n_{13}$ between 3 and 14 of Zn_3Sn_1 and Zn_1Sn_3 motifs ("31 disorder") per 128-atom supercell, corresponding to $0.05 \leqslant x \leqslant 0.22$. Note that the minimum number $n = 3$ is obtained when creating a single exchange defect $Zn_{Sn} + Sn_{Zn}$ between two close cation sites that share a nitrogen neighbor, whereas an exchange defect between distant cation sites results in $n = 4$. We confirmed that the calculated DFT energies are in good approximation proportional to the fraction $x_{31} = x_{13}$, thereby validating the applicability of the model Hamiltonian [Eq. (1)]. Since, as we will show below, the electronic properties are insensitive to octet-rule conserving disorder, and since the formation of Zn_4 and Sn_4 motifs is unfavorable (Fig. 1), we will use the fraction $x_{31} = x_{13}$ as an order parameter to describe the evolution of the properties of stoichiometric $ZnSnN_2$ as a function of cation disorder. For comparison purposes, we further selected five Monte Carlo samples containing a Zn_4 motif and five samples containing a Sn_4 motif. In these cases, the stoichiometry is maintained by varying ratios of Zn_3Sn_1 and Zn_1Sn_3 motifs. Finally, we generated five samples of fully randomized cation distributions in the same 128-atom cell size. These random structures, which include Zn_4 and Sn_4 motifs, are on average 83 ± 13 meV/atom above the ground state. For comparison, the supercells with 31 disorder at a concentration of $n_{31} = 6$ ($x_{31} = 0.09$) have an energy of 17 ± 1 meV/atom.

In Fig. 2, we compare the x-ray diffraction (XRD) patterns of a $ZnSnN_2$ sample grown by sputtering with the simulated spectra based upon the atomic structure models discussed above. The experimental sample was grown at 200 °C using 5% H_2 balanced by N_2 as the nitrogen source. It has a thickness of 500 nm, and the cation stoichiometry of $Zn/(Zn + Sn) = 0.50$ was confirmed by x-ray fluorescence. Please see Ref. [19] for details on the thin-film deposition. A full width at half maximum of 0.2° in 2θ was used in the simulated patterns. Note that the first decade in the measured spectrum is subject to uncertainties due to subtraction of the background intensity from the amorphous glass substrate. (The raw data and baseline

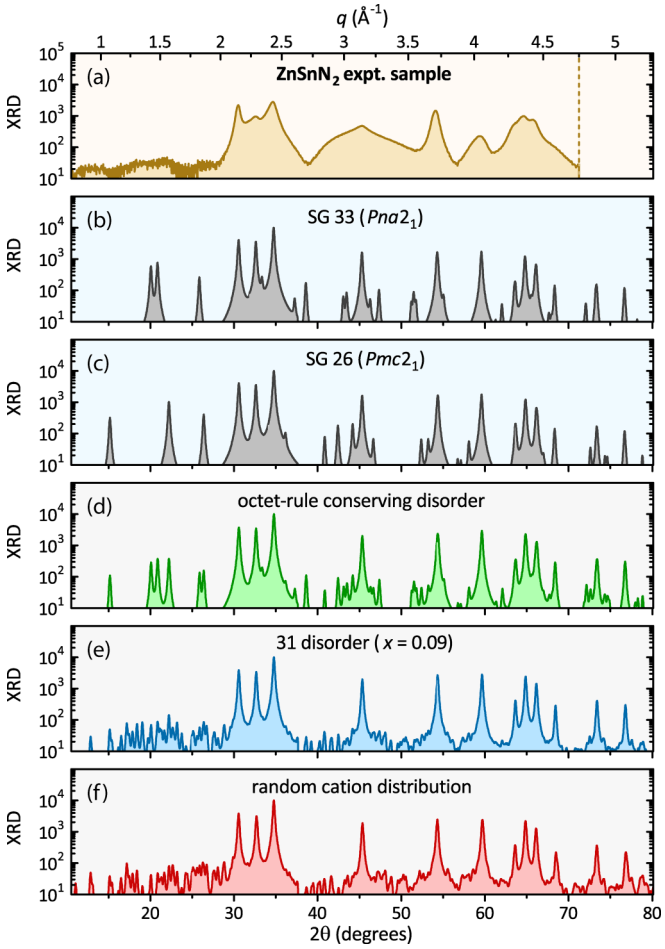

FIG. 2. (a) Measured x-ray diffraction of a $ZnSnN_2$ sample grown by sputtering as a function of scattering vector q (top axis, data taken at $\lambda = 0.9744$ Å). The vertical dashed line marks the end of measurement range. (b), (c) Simulated XRD of ordered orthorhombic unit cells with space groups 33 and 26. (d)–(f) Simulated XRD of disordered 128-atom cells. The q and 2θ axes are scaled for equidistant spacing in 2θ (bottom) using the Cu $K\alpha$ standard ($\lambda = 1.5406$ Å).

construction is shown in Fig. S1 in the Supplemental Material [21].) An XRD pattern close to that of a perfect wurtzite structure would be expected for a fully randomized distribution of Zn and Sn cations [Fig. 2(f)]. The experimental spectrum [Fig. 2(a)], taken using a synchrotron source to maximize signal to noise, clearly shows all features expected for a wurtzite lattice. On the other hand, the cation ordering in the small unit cells of the SG33 and SG26 crystal structures would give rise to additional features, most notably in the low-angle region around $2\theta = 15°$, 20°, and 26° (referring to the Cu $K\alpha$ standard with $\lambda = 1.5406$ Å). These features are not observed in the experimental data. [Please see also Fig. S2 in the Supplemental Materials for the two-dimensional (2D) resolved XRD data.] The simulated XRD for strictly octet-rule conserving disorder [Fig. 2(d)] results in a pattern that preserves and combines the features of the orthorhombic 8- and 16-atom primitive cells. However, the simulations also show that already a moderate degree of octet-rule violating 31 disorder [Fig. 2(e)] leads to patterns that are essentially indistinguishable from a fully randomized structure [Fig. 2(f)]. From the absence of any discernible features in the range $q = 1-1.9$ Å^{-1} ($2\theta = 15°-26°$) in the measured spectrum, we can conclude that our experimental samples are likely to contain at least some degree of octet-rule violating disorder. Since the XRD patterns are rather insensitive to a further increase of the level of disorder, additional measurement techniques that are more sensitive to the local chemical environments, such as x-ray absorption and extended x-ray absorption fine structure, might be helpful to characterize disorder in $ZnSnN_2$ in the future.

The unambiguous identification of the fully ordered ground state by XRD is difficult in $ZnSnN_2$, since lattice parameters remain very close to those of a wurtzite lattice. Specifically, we find that the calculated c/a and b/a ratios of the orthorhombic SG 33 and SG 26 cells deviate by less than 0.5% from those for an ideal wurtzite supercell, i.e., $c/a = \sqrt{8/3}$, $b/a = \sqrt{4/3}$ (SG 33), and $b/a = \sqrt{3}$ (SG 26). In contrast, the deviation from a wurtzite lattice in $ZnGeN_2$ is much larger, thereby allowing a more direct access to ordering effects [20]. We further find that the lattice volume slightly increases with increasing disorder, with the largest change about +0.4% in the linear lattice parameters obtained for the fully random cation distribution. Thus, the variation of lattice parameters with growth temperature, as recently reported in Refs. [18,22], does not seem to be a direct consequence of ordering. The breaking of the hexagonal symmetry in the basal plane, which was also observed in these works, might be a consequence of the reduction of the octet-rule violating disorder. However, due to the very close energies of all octet-rule conserving structures (see above), our present calculations question the feasibility of obtaining the fully ordered ground-state structure (SG 33) via thermal protocols. On the other hand, the octet-rule conserving disorder allows only very specific cation arrangements [13], which, as we show below, share most properties with the ordered orthorhombic structures.

Spatial correlations of octet-rule violating motifs. An interesting aspect of the results of the MC simulations is the observation of a continuous phase transition (Fig. 1). Within the exchange defect model [10], one would expect a simple exponential increase of defects with temperature. An initial exponential increase in x_{31} is indeed observed in our MC simulations up to about 1600 °C. However, with an increasing degree of disorder, the exchange defects can no longer form independently, as they are subject to constraints such as the requirement to avoid energetically costly Zn_4 and Sn_4 motifs. As a result, the order parameter already deviates from the exponential increase at around $x_{31} = 0.02$ and eventually saturates at around $x_{31} = 0.2$ (Fig. 1). At the same time, the enthalpy is, in good approximation, described as a linear function of x_{31} up to and beyond $x_{31} = 0.2$. Thus, the phase transition results from the effects of the configurational entropy rather than the enthalpy. Indeed, the topological constraints requiring that the disordered cation arrangement forms in such a way to avoid high-energy motifs leads to spatial correlations in the motif distribution, and give rise to interesting physical phenomena such as entropy-driven clustering observed in the simulation of Cu_2SnS_3 and Cu_2ZnSnS_4 [9].

In order to characterize possible motif-clustering effects in $ZnSnN_2$, we analyzed the mutual coordination of the N-centered Zn_3Sn_1 and Zn_1Sn_3 motifs, similarly as done in

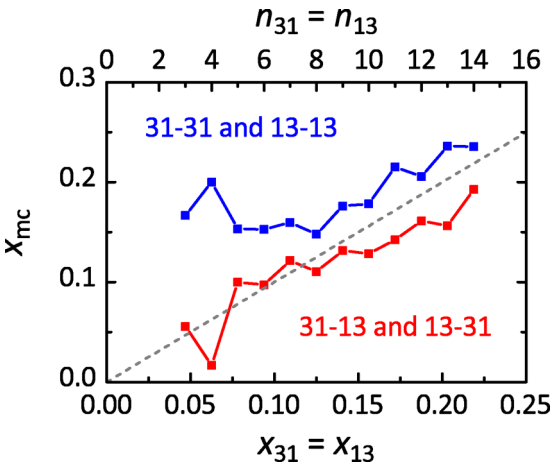

FIG. 3. The correlation of octet-rule violating Zn_3Sn_1 and Zn_1Sn_3 motifs as a function of the cation disorder, obtained from the Monte Carlo samples. The fraction x_{mc} gives the average coordination of a Zn_3Sn_1 or a Zn_1Sn_3 motif with one of the same or opposite type. The dashed line corresponds to the uncorrelated random limit.

Ref. [9] for the ternary and quaternary chalcogenides. In the wurtzite structure, the anion site is coordinated by 12 next-nearest-neighbor anions. In disordered $ZnSnN_2$, each octet-rule violating motif, e.g., Zn_3Sn_1, is coordinated by a certain number m_{31} of same-type (Zn_3Sn_1) and m_{13} of opposite-type (Zn_1Sn_3) motifs. Figure 3 shows the corresponding motif coordination (mc) fractions $x_{mc}(31\text{-}31) = \langle m_{31}/12 \rangle$ and $x_{mc}(31\text{-}13) = \langle m_{13}/12 \rangle$, where the brackets indicate that the average is taken. In the absence of Zn_4 and Sn_4 motifs, we further have $x_{mc}(31\text{-}31) = x_{mc}(13\text{-}13)$ and $x_{mc}(31\text{-}13) = x_{mc}(13\text{-}31)$. In the hypothetical limit of uncorrelated, randomly distributed motifs, any N site would be coordinated in proportion to the respective motif concentration, e.g., $x_{mc}(31\text{-}31) = x_{31}$; larger values of x_{mc} indicate clustering, lower values anticlustering. The pronounced clustering of same-type motifs seen in Fig. 3 in the low-concentration limit is a simple consequence of the fact that individual cation exchange defects create groups of three or four octet-rule violating motifs, as discussed above. At higher concentrations, we observe only a modest clustering effect between same-type motifs ($x_{mc} > x_{31}$) and a modest anticlustering effect of opposite-type motifs ($x_{mc} < x_{31}$). Due to the similarity of x_{mc} to the uncorrelated random limit (Fig. 3), we do not expect in $ZnSnN_2$ strong clustering-induced potential fluctuations as found, e.g., for Cu_2ZnSnS_4 [9], thereby ruling out an important potential drawback of multinary photovoltaic materials.

Electronic structure and optical properties. The magnitude of the band gap of ordered, orthorhombic $ZnSnN_2$ is not well established in the literature. Experimentally, it is difficult to eliminate the effects of disorder, off-stoichiometry, and degenerate doping that can cause a Burstein-Moss shift. Experimental band-gap measurements range from approximately 1 to 2 eV [4,5,8,17], and calculated results also vary over a somewhat wider range. An overview of both the computational and experimental literature on $ZnSnN_2$ and related II-IV-V_2 materials is given in a recent review article [23]. Computational results based on standard DFT or hybrid functionals [4,8] are hardly predictive due to the strong dependence on the hybrid functional parameters. More meaningful predictions can be obtained from many-body perturbation theory in the GW approximation [24], although even here, the results can depend somewhat on the details of the approach. We use here the results of GW calculations from the NREL materials database [25] (please see Refs. [26,27] for computational details), with $E_g = 1.41$ eV for $ZnSnN_2$ in the SG 33 ground state. This band gap is somewhat smaller than $E_g = 1.81$ eV obtained in the GW approach of Ref. [13]. For comparison, the uncorrected DFT band gap is only 0.13 eV, increasing to $E_g = 2.09$ eV [8] for a hybrid functional with a standard value of $\alpha = 0.25$ for the fractional Fock exchange. It is also important to note that $ZnSnN_2$ is a piezoelectric material, which can have device implications at a photovoltaic *pn* junction [28]. The piezoelectric coefficients, calculated at the DFT + U level for the SG33 structure, are $e_{33} = 0.68\,\mathrm{C/m^2}$ and $e_{13} = -0.35$, lying between the values for GaN ($e_{33} = 0.41$; $e_{13} = -0.26$) and ZnO ($e_{33} = 1.01$; $e_{13} = -0.50$).

For the large 128-atom supercells generated by the MC simulation for disordered $ZnSnN_2$, the direct application of the GW approach is not feasible. Therefore, we employ a simpler parameterized single-shot hybrid $+U$ (SSH + U) functional to calculate the electronic structure in the supercells. The SSH + U parameters are adjusted such to reproduce results of the GW calculation for the orthorhombic ground state, which yields $\alpha = 0.14$ and $U = 4$ eV for the on-site Coulomb parameter in the Zn-3*d* shell. As indicated by the term "single-shot," the wave functions of the initial DFT + U calculation are kept fixed, thereby avoiding the computationally costly but unessential diagonalization of the hybrid functional Hamiltonian. Note that the combination of Fock exchange and DFT + U is important to obtain correctly both the band gap and the energy of the Zn-3*d* orbitals [26]. Comparing the density of states (DOS) of $ZnSnN_2$ in the ordered SG 33 structure between the original GW calculation and the parameterized SSH + U functional, we observe practically perfect agreement across the full energy spectrum, even on an absolute energy scale without any need for alignment (see Fig. S3 in the Supplemental Material). The following results were obtained using the SSH + U functional.

The calculated dependence of the $ZnSnN_2$ band gap on the order parameter x_{31} is shown in Fig. 4(a). We observe that the octet-rule conserving disorder ($x_{31} = x_{13} = 0$) has a negligible effect on the band structure, in agreement with the recent work in Ref. [13]. With increasing disorder, we observe a reduction of E_g to about 1.1 eV at $x_{31} = 0.1$. The calculated optical absorption spectra in Fig. 4(b) also reflect the band-gap reduction and show a slightly slower absorption onset above E_g when compared to perfect cation ordering or octet-rule conserving disorder. Supercell representations of fully randomized cation disorder were evaluated for comparison, even though these structures are energetically unfavorable. Similar to Ref. [8], we find a band-gap reduction in the order of 1 eV but with a large variance. In random cation representations, which contain Zn_4 and Sn_4 motifs, the gap sometimes closes entirely.

An experimental absorption spectrum is also shown in Fig. 4(b). This sample was grown under similar conditions as those of the sample used for XRD in Fig. 2(a), except that the nitrogen source was pure N_2 with no added hydrogen.

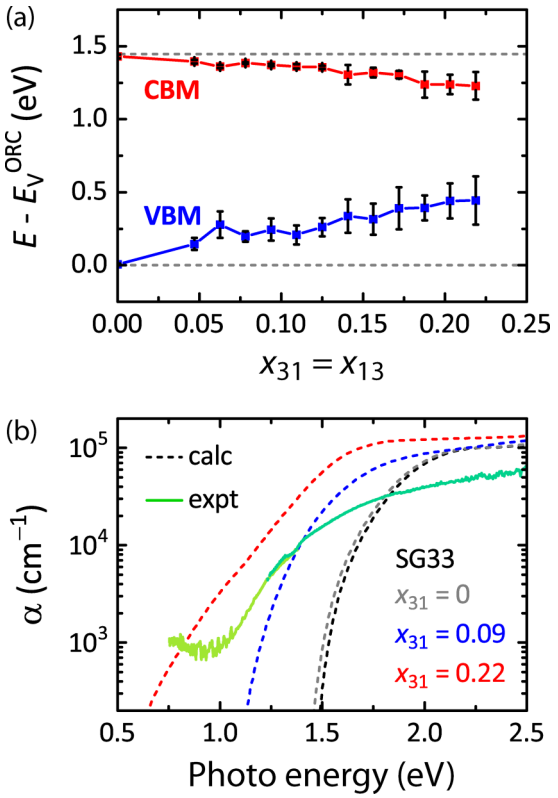

FIG. 4. (a) Dependence of the band gap on the order parameter x_{31}. (b) Solid line: Experimental absorption spectrum in Zn-rich $ZnSnN_2$. Dashed lines: Calculated absorption spectrum for $ZnSnN_2$ in the fully ordered (SG 33) structure, the octet-rule conserving disorder ($x_{31} = 0$), and for different degrees of 31 disorder.

The sample thickness is 530 nm. For measurement of the optical properties, we are using a Zn-rich composition with $Zn/(Zn + Sn) = 0.67$. Whereas stoichiometric $ZnSnN_2$ is often degenerately doped with carrier densities in the order of $n = 10^{20}$–10^{21} cm^{-3} [4,8], the increased Zn composition enables the reduction of the free electron concentration [5,19] down to $n = 10^{18}$ cm^{-3} for the present sample. This electron concentration is sufficiently low to avoid an artificially increased energy for the absorption onset due to the Burstein-Moss shift (ΔE_{BM}) [29,30]. From the electron effective mass and conduction band density of states obtained in the GW calculations, we estimate $\Delta E_{BM} = 0.02$ eV. [Please see Fig. S4 in the Supplemental Materials for the function $\Delta E_{BM}(n)$.] Comparing the measured absorption spectrum with those for different computational models, we see in Fig. 4(b) that the absorption threshold agrees well with an intermediate level of disorder of around $x_{31} \approx 0.1$. Thus, a band-gap reduction of 0.3–0.4 eV due to disorder is plausible. It is notable that in the related zinc-blende-derived ternary compound $ZnSnP_2$, a similar variation of the band gap was observed as a result of different cooling rates affecting the long-range ordering [31]. However, we also note that a direct comparison between the measurements and disorder models in $ZnSnN_2$ is difficult due to the off-stoichiometric Zn/Sn ratio and a certain level of O incorporation. A more detailed comparison will require incorporating these effects into the atomic structure models in the future.

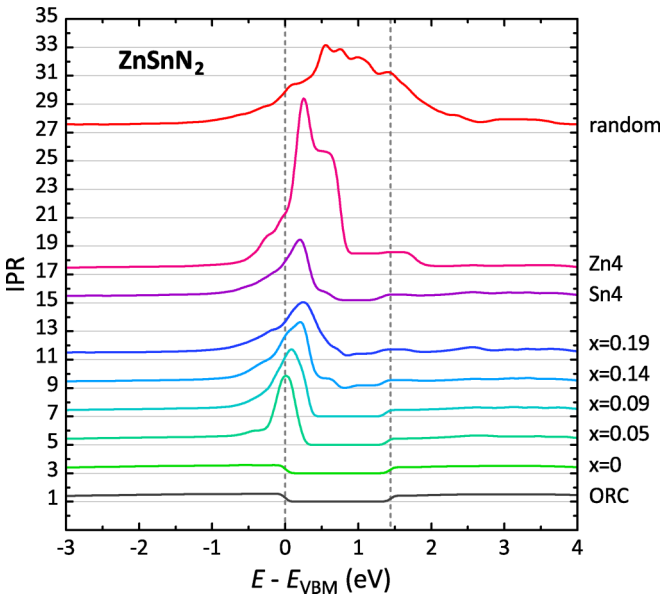

FIG. 5. Inverse participation ratio IPR(E) in $ZnSnN_2$ for perfect ordering (SG 33), for various values of the x_{31} order parameter, for supercell representations containing Zn_4 and Sn_4 motifs, and for fully randomized cation disorder.

Disorder-induced electron localization. The next important question we address computationally is how disorder is expected to affect the carrier transport properties. Disorder-induced localization of the electronic states at the valence or conduction band edges is undesirable, as it will hamper charge collection in a solar cell. In order to quantify the degree of localization, we calculated the inverse participation ratio, defined as

$$\mathrm{IPR}(E) = \frac{N \sum_i p_i(E)^2}{\left(\sum_i p_i(E)\right)^2}, \tag{2}$$

where E is the energy, p_i is the atom-projected local density of states (LDOS), and i is the index running over the N atoms in the cell. The inverse participation ratio (IPR) measures the inverse fraction of atoms contributing to the DOS, i.e., the sum of the atomic LDOS, at a given energy. For example, IPR = 1 would indicate a perfectly even distribution of the density of states among all atoms, i.e., complete delocalization, whereas IPR = 10 implies that an electronic state is on average localized on one out of ten atoms. Figure 5 shows the IPR for ordered ORC $ZnSnN_2$, for various values of x_{31}, for supercell representations containing Zn_4 and Sn_4 motifs, and for fully randomized cation distributions. (Note that the Zn_4 structures also contain Zn_1Sn_3 motifs and the Sn_4 structures contain Zn_3Sn_1 motifs so as to maintain the $Zn_1Sn_1N_2$ stoichiometry.) We observe an IPR close to 1 for perfectly ordered $ZnSnN_2$ and for octet-rule conserving disorder, again highlighting the benign nature of the latter. The formation of Zn_3Sn_1 and Zn_1Sn_3 motifs causes some localization effects around the valence-band maximum, but the conduction band remains essentially unperturbed. The maximal value of the IPR is around 4, indicating only moderate localization effects. For comparison, a $Cu_{Zn} + Zn_{Cu}$ exchange defect in Cu_2ZnSnS_4 creates an IPR of about 3 at the valence-band edge.

A strong localization with IPR ≈ 10 is observed for the Zn_4 motif. These localization effects can be understood by the hybridization of N-p with Zn-d orbitals, creating antibonding states that increase in energy for higher Zn coordination of nitrogen atoms. This interpretation also explains the marked upward shift of the valence-band maximum energy with increasing x_{31} disorder [Fig. 4(a)]. In contrast, the higher Sn coordination of nitrogen in Sn_4 motifs does not cause additional localization effects. Finally, full randomization essentially creates a continuum of defect states throughout the band-gap region, consistent with the predicted closing of the band gap for highly disordered $ZnSnN_2$, as mentioned above in the discussion of the electronic structure.

Methods. DFT, GW, and hybrid functional calculations were performed using the VASP code with the respective implementations in the projector augmented wave (PAW) method [32–34]. The generalized gradient approximation (GGA) of Ref. [35] was used for DFT exchange correlation. For the simulation of XRD (Fig. 2), the tendency of GGA to overestimate lattice parameters was compensated by an isotropic reduction of the lattice constants by 1%. In determining the parameters for the SSH + U functional, we found that the best fit was obtained with a range-independent hybrid functional [36], and the DFT + U formulation of Ref. [37] was used. The 128-atom supercells used as a basis for the disordered configurations were obtained by doubling of the lattice vectors of the 16-atom primitive cell of ORC $ZnSnN_2$. Brillouin-zone sampling was performed on a $4 \times 4 \times 4$ Γ-centered k mesh. The piezoelectric coefficients were calculated within the PAW implementation of density functional perturbation theory [38] at the GGA + U level ($U = 6$ eV for Zn-d).

Two-dimensionally resolved, wide-angle x-ray scattering (WAXS) was measured at the Stanford Synchrotron Radiation Lightsource (SSRL) beamline 11-3 at an x-ray energy of 12.7 keV ($\lambda = 0.9744$ Å), using a Rayonix CCD detector. The data were collected in the grazing incidence geometry with an incidence angle of 3°. The images were calibrated using a LaB_6 standard and integrated between polar angles $10^\circ < \chi < 170^\circ$ using GSAS-II [39]. The samples were slightly oriented or textured, which can be seen in the two-dimensional (2D) image (Fig. S2), but there were no low-angle peaks present that would be outside of the integration limits used to reduce the data presented in Fig. 2(a). The experimental absorption spectrum in Fig. 4(b) was taken using a mapping-style UV-visible near-infrared thin-film optical spectroscopy system covering the 300–2000 nm spectral range. More details on the experimental method used to collect the spectrum can be found in Ref. [5].

Conclusions. We performed Monte Carlo simulations of disorder in stoichiometric $ZnSnN_2$ and found that thin-film growth is likely to result in degrees of cation disorder lying between the extreme limits of full cation randomization and the ordered ground-state structure. Partial disorder that does not disrupt the octet-rule conserving Zn_2Sn_2 coordination of N occurs readily with exceedingly small energy differences in the order of 1 meV/atom. Therefore we expect that full, long-range ordering in the 16-atom primitive cell of the orthorhombic (SG 33) ground-state crystal structure is very difficult to realize experimentally. The next level of disorder, involving the formation of octet-rule violating Zn_3Sn_1 and Zn_1Sn_3 motifs at an energy cost of up to around 20 meV/atom is likely to occur under nonequilibrium growth conditions, but careful equilibration could possibly reduce or even eliminate these non-ground-state motifs. Disorder involving the formation of Zn_4 and Sn_4 motifs is energetically too costly to occur at significant levels, even under nonequilibrium conditions. Simulation of the XRD patterns resulting from the different degrees of disorder suggests that even moderate levels of octet-rule violating motifs will result in the appearance of a wurtzite-like pattern, essentially indistinguishable from a random cation distribution. Despite the loss of long-range order, octet-rule conserving disorder retains weak nonwurtzite features that could possibly be resolved. Characterized by synchrotron measurements, our $ZnSnN_2$ thins films grown by sputtering did not exhibit nonwurtzite features, indicating at least some degree of cation disorder involving octet-rule violating motifs. Techniques focused on measuring the local chemical environments, rather than long-range order, will be better suited to resolve differences in the cation ordering.

The electronic properties, notably, seem to be determined primarily by the changes of the *local* coordination environments rather than *long-range* ordering effects. Our first-principles calculations suggest that full randomization would be very detrimental to the electronic structure, whereas strictly octet-rule conserving disorder would be perfectly benign. For realistic degrees of disorder, we expect the formation of Zn_3Sn_1 and Zn_1Sn_3 motifs at concentrations around $x_{31} \approx x_{13} \approx 0.1$, leading to a moderate band-gap reduction of about 0.3 eV and moderate localization effects at the valence-band edge. Our experimentally measured optical absorption data is consistent with this prediction, but additional studies on off-stoichiometric Zn/Sn compositions are desirable. The variation of cation ordering among different experimental samples, combined with the Burstein-Moss shift, can explain experimentally observed variations in the band gap.

Acknowledgments. This work was supported by the US Department of Energy (DOE), Office of Energy Efficiency and Renewable Energy, under Contract No. DE-AC36-08GO28308 to the National Renewable Energy Laboratory (NREL). Work by A.T. was supported by the DOE, Office of Science (SC), Basic Energy Sciences (BES), Materials Sciences and Engineering Division. This work used computational resources sponsored by the Department of Energy's Office of Energy Efficiency and Renewable Energy, located at NREL. Use of the Stanford Synchrotron Radiation Lightsource, SLAC National Accelerator Laboratory, is supported by DOE-SC-BES under Contract No. DE-AC02-76SF00515.

[1] S. Siebentritt, M. Igalson, C. Persson, and S. Lany, Prog. Photovolt: Res. Appl. **18**, 390 (2010).

[2] A. Polizzotti, I. L. Repins, R. Noufi, S.-H. Wei, and D. B. Mitzi, Energy Environ. Sci. **6**, 3171 (2013).

[3] N. Feldberg, B. Keen, J. D. Aldous, D. O. Scanlon, P. A. Stampe, R. J. Kennedy, R. J. Reeves, T. D. Veal, and S. M. Durbin, *Proceedings of the 38th IEEE Photovoltaic Specialists Conference (PVSC)* (IEEE, New York, 2012), p. 2524.
[4] L. Lahourcade, N. C. Coronel, K. T. Delaney, S. K. Shukla, N. A. Spaldin, and H. A. Atwater, Adv. Mater. **25**, 2562 (2013).
[5] A. N. Fioretti, A. Zakutayev, H. Moutinho, C. Melamed, J. D. Perkins, A. G. Norman, M. Al-Jassim, E. S. Toberer, and A. C. Tamboli, J. Mater. Chem. C **3**, 11017 (2015).
[6] M. A. Ryan, M. W. Peterson, D. L. Williamson, J. S. Frey, G. E. Maciel, and B. A. Parkinson, J. Mater. Res. **2**, 528 (1987).
[7] P. F. Ndione, Y. Shi, V. Stevanovic, S. Lany, A. Zakutayev, P. A. Parilla, J. D. Perkins, J. J. Berry, D. S. Ginley, and M. F. Toney, Adv. Funct. Mater. **24**, 610 (2014).
[8] N. Feldberg, J. D. Aldous, W. M. Linhart, L. J. Phillips, K. Durose, P. A. Stampe, R. J. Kennedy, D. O. Scanlon, G. Vardar, R. L. Field III, T. Y. Jen, R. S. Goldman, T. D. Veal, and S. M. Durbin, Appl. Phys. Lett. **103**, 042109 (2013).
[9] P. Zawadzki, A. Zakutayev, and S. Lany, Phys. Rev. Appl. **3**, 034007 (2015).
[10] D. Skachkov, P. C. Quayle, K. Kash, and W. R. L. Lambrecht, Phys. Rev. B **94**, 205201 (2016).
[11] S. Chen, J.-H. Yang, X. G. Gong, A. Walsh, and S.-H. Wei, Phys. Rev. B **81**, 245204 (2010).
[12] A. Zunger, S. H. Wei, L. G. Ferreira, and J. E. Bernard, Phys. Rev. Lett. **65**, 353 (1990).
[13] P. C. Quayle, E. W. Blanton, A. Punya, G. T. Junno, K. He, L. Han, H. Zhao, J. Shan, W. R. L. Lambrecht, and K. Kash, Phys. Rev. B **91**, 205207 (2015).
[14] D. J. Thouless, Phys. Rep. **13**, 93 (1974).
[15] W. R. L. Lambrecht, E. Alldredge, and K. Kim, Phys. Rev. B **72**, 155202 (2005).
[16] S. Lany, Phys. Rev. B **78**, 245207 (2008).
[17] P. C. Quayle, K. He, J. Shan, and K. Kash, MRS Communications **3**, 135 (2013).
[18] R. A. Makin, N. Senabulya, J. Mathis, N. Feldberg, P. Miska, R. Clarke, and S. M. Durbin, J. Vac. Sci. Technol. B **35**, 02B116 (2017).
[19] A. N. Fioretti, A. Stokes, M. R. Young, B. Gorman, E. S. Toberer, A. C. Tamboli, and A. Zakutayev, Adv. Electron. Mater. **3**, 1600544 (2017).
[20] E. W. Blanton, K. He, J. Shan, and K. Kash, J. Cryst. Growth **461**, 38 (2017).
[21] See Supplemental Material at http://link.aps.org/supplemental/10.1103/PhysRevMaterials.1.035401 for additional data pertaining to the XRD analysis, the band-gap-corrected SSH + U calculations, and the carrier density dependence of the Burstein-Moss shift.
[22] N. Senabulya, N. Feldberg, R. A. Makin, Y. Yang, G. Shi, C. M. Jones, E. Kioupakis, J. Mathis, R. Clarke, and S. M. Durbin, AIP Adv. **6**, 075019 (2016).
[23] A. D. Martinez, A. N. Fioretti, E. S. Toberer, and A. C. Tamboli, J. Mater. Chem. A, **5**, 11418 (2017).
[24] L. Hedin, Phys. Rev. **139**, A796 (1965).
[25] https://materials.nrel.gov
[26] L. Y. Lim, S. Lany, Y. J. Chang, E. Rotenberg, A. Zunger, and M. F. Toney, Phys. Rev. B **86**, 235113 (2012).
[27] S. Lany, Phys. Rev. B **87**, 085112 (2013).
[28] M. Mitra, J. Drayton, M. L. C. Cooray, V. G. Karpov, and D. Shvydka, J. Appl. Phys. **102**, 034505 (2007).
[29] E. Burstein, Phys. Rev. **93**, 632 (1954).
[30] T. S. Moss, Proc. Phys. Soc. London Sect. B **67**, 775 (1954).
[31] S. Nakatsuka and Y. Nose, J. Phys. Chem. C **121**, 1040 (2017).
[32] G. Kresse and D. Joubert, Phys. Rev. B **59**, 1758 (1999).
[33] M. Shishkin and G. Kresse, Phys. Rev. B **74**, 035101 (2006).
[34] J. Paier, R. Hirschl, M. Marsman, and G. Kresse, J. Chem. Phys. **122**, 234102 (2005).
[35] J. P. Perdew, K. Burke, and M. Ernzerhof, Phys. Rev. Lett. **77**, 3865 (1996).
[36] J. P. Perdew, M. Ernzerhof, and K. Burke, J. Chem. Phys. **105**, 9982 (1996).
[37] S. L. Dudarev, G. A. Botton, S. Y. Savrasov, C. J. Humphreys, and A. P. Sutton, Phys. Rev. B **57**, 1505 (1998).
[38] M. Gajdos, K. Hummer, G. Kresse, J. Furthmuller, and F. Bechstedt, Phys. Rev. B **73**, 045112 (2006).
[39] B. H. Toby and R. B. Von Dreele, J. Appl. Crystallogr. **46**, 544 (2013).